Electronic Supplementary Material (ESI) for Soft Matter.

Liquid Interfaces with pH-switchable Nanoparticle Arrays

Sunita Srivastava[1,2], Masafumi Fukuto[3] and Oleg Gang[2,4,5]*

[1]Department of Physics, Indian Institute of Technology Bombay, Mumbai 400076, India.

[2]Center for Functional Nanomaterials, Brookhaven National Laboratory, Upton, NY, 11973, USA.

[3]Condensed Matter Physics and Materials Science Department and National Synchrotron Light Source II, Brookhaven National Laboratory, Upton, NY, 11973, USA.

[4]Department of Chemical Engineering, Columbia University, New York, NY, 10027, USA

[5]Department of Applied Physics and Applied Mathematics, Columbia University, New York, NY, 10027, USA

Keywords: Self-assembly, Responsive nanostructures, Liquid interfaces, DNA, Nanoparticles

I. Material and Methods. The charged interfaces were prepared by depositing a monolayer composed of cationic lipids at water surface by the Langmuir technique[1]. The cationic lipids, 1,2-dimyristoyl-3-trimethylammonium-propane (DMTAP) were purchased from Avanti Polar Lipids, Inc. The NPs of were purchased from Ted Pella. Gold nanoparticles were functionalized with ssDNA (Integrated DNA technologies) (see Table 1 below), using the protocol described elsewhere [2]. All other chemicals used in this study were purchased from Sigma Aldrich. Ultrapure water (Millipore, 18.2 MΩ-cm) was used throughout sample preparation.

The home-built Teflon troughs with a fixed area of 2535 mm^2 were used for 2D sample preparation[1, 3]. The trough was equipped with a delrin port for injection of gold nanoparticle solution into the subphase without disturbing the lipid monolayer. The trough held 9 ml of sub phase (water). The in-situ GISAXS and XRR measurements were carried out at the X22 beam line of the National Synchrotron Light Source (NSLS), using an X-ray energy of 8.2 keV. The GISAXS data were collected using an area detector (Princeton Instruments) located 1 m from the sample center. For the X-ray measurements, the trough was enclosed in an aluminum box filled with humidified helium, which helped to reduce the background scattering and radiation-induced oxidation. The measurements were taken at constant temperature of 23 ^oC that was controlled by circulating water through the plate underneath the trough. In a typical experiment ~ 60 μL of 0.1 mM lipid solution was spread on the water surface using a Hamilton syringe to form a fluid-like monolayer with an average molecular area of ~ 75 $Å^2$/lipid. After an equilibration time of 30- 40 min, a solution of DNA-coated gold NPs in water (typically 250 uL at ~ 200 nM) was injected into the sub phase through the injection port. Upon adding NPs, 2D assembly instantaneously initiated at the interface due to the electrostatic attractive interactions between DNA and the positively charged head group of the cationic lipid as evidenced by enhanced scattering intensities in the in-plane scattering measurements. After equilibration for ~ 3-4 hrs, the final scattering data were collected in-situ to study the structure of the 2D assemblies. The methodology for formation of pH dependent DNA-NP assemblies is discussed in main text.

Table ST1: The DNA sequence design (5' to 3' direction) for system presented in paper. HSC_6H_{12} represents the thiol modification. The linker DNA sequence comprises of total "*n (=18, 28, 36)*" bases of A nucleotide which can form *A* motif at acidic pH.

Thiolated DNA chains	HSC_6H_{12}- TTGGCTGCGTTGGCTGGATAGCTGTGTTCTTAACCTAACCGGCAG
Linker (*n*)	$(A)_n$ CTGCCGGTTAGGTTG
Control Linker	$(T)_n$ CTGCCGGTTAGGTTG

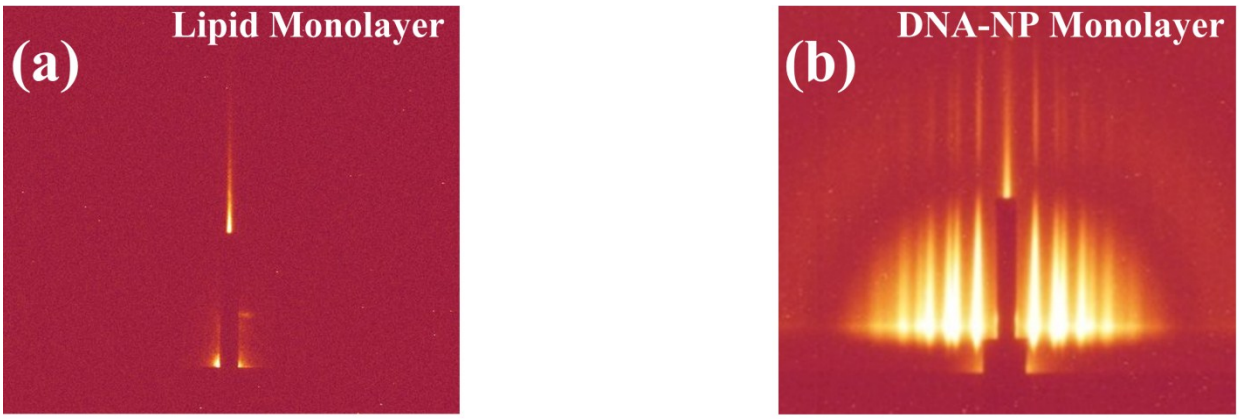

Figure S1. GISAXS data from neutral lipid monolayer with 100% composition of cationic lipid and for system with added DNA-NP solution in the sub-phase. To note the absence of Brag diffraction peak for neutral lipid monolayer confirms that cationic lipid facilitates the adsorption of DNA-NP to the interface through electrostatic attraction. Presence of brag diffraction rods in (b) reveals formation of long ordered NP arrays at the lipid interface (refer main text).

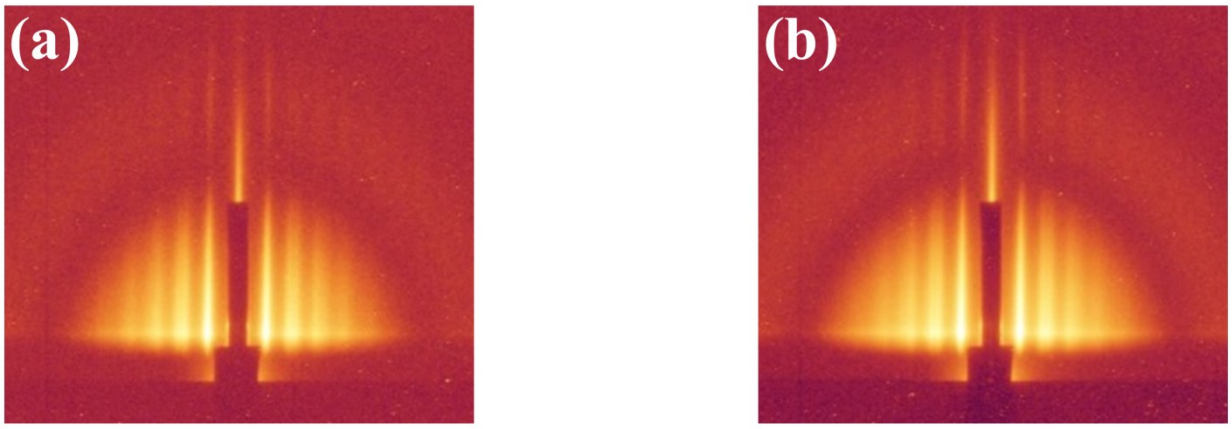

Figure S2. GISAXS data for control experiments containing DNA linkers rich in poly (T) (n=28), for (a) pH 7.4 and (b) pH 3.5. As evident from the data, the T-rich DNA linkers do not exhibit the change in structural features, which were observed for *A*-rich linker (as shown in the main text). This confirms that the structural changes observed in our *A*-rich DNA linker systems are driven by the pH-mediated formation of *A*-motif (see main text) at acidic pH.

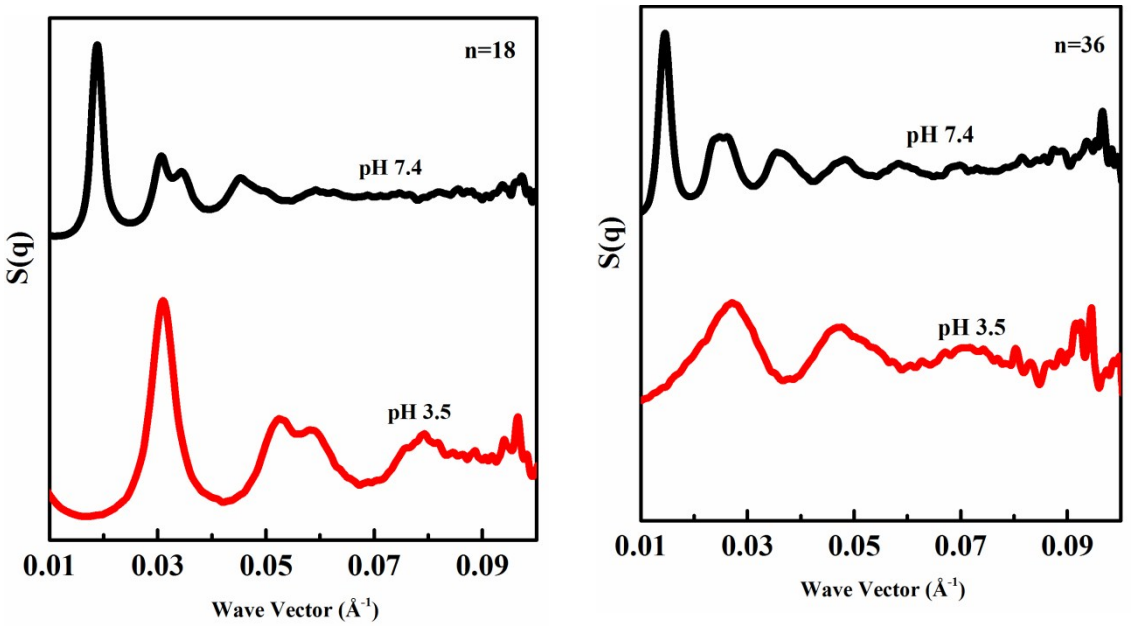

Figure S3. Structure factor, S(q), extracted from GISAXS data (refer main text) for n=18 (a) and 36 (b) at pH=7.4 and pH=3.5. Note the shift in the first diffraction peak when pH is changed from 7.4 to 3.5, indicating the switch from expanded to contracted lattice.

II. In-situ x-ray reflectivity at the interface

We performed simultaneous in-situ x-ray reflectivity (XRR) measurements along with GISAXS to investigate the structural evolution of the NP monolayer normal to the surface (Figure 3, main text). The angular settings for XRR measurements were adjusted around critical angle of water for maximum total external reflectivity signal. Measured data from lipid and DNA-NP layer along with fitted data is shown in Figure S4. The XRR for lipid monolayer exhibits a minima at the high normal wave vector ~ 0.3Å^{-1}, corresponding to the thickness of the lipid monolayer (Figure S4a). In contrast strong oscillations at low normal wave vector appear in the XRR profile on addition of nanoparticles due to the scattering from adsorbed gold nanoparticles at the interface (Figure 3a, main text). The period and amplitude of these oscillations are related to the thickness and density of the adsorbed DNA-NP monolayer. The reflectivity curves were fitted with Igorpro (Wavemetrics, Inc.) using package Motofit[4]. To extract average normal electron density profile we fit XRR data using model based on Parratt algorithm consisting of m boxes for different layers and interfaces. In this model, each layer between the aqueous subphase and vapor interface is assigned a box and interfaces are smeared out by a Gaussian roughness. For example, we fit the XRR data for lipid monolayer with three box model, first two boxes account for the head group, hydrocarbon chains of the lipid molecules respectively and the third box accounts for roughness at the lipid water interface (Figure S4b). The model for analysing XRR from DNA-NP layer comprises of additional boxes accounting for, DNA chains in vicinity of the surface along with a separate box for gold nanoparticles. Roughness between the lipid and nanoparticle layer was allowed to vary to account for any inhomogeneity of the monolayer. We first fit lipid layer with no absorbed nanoparticles at the interface. The parameters obtained from this fit for lipid layer were kept fixed for all DNA nanoparticle systems. In some cases, we allow the roughness to vary for a better fit, however, the obtained values did not differ significantly. The electron density profiles are consistent with the presence of a DNA-NP layer underneath a monolayer of lipid molecules at the air-water interface, with their low density tail pointing towards the air and the high density head group towards the sub phase. We estimate the maximum value of the electron density of lipid layer, ρ_l ~ 0.35e/Å$^{3.}$ This value is higher than that of water (~ 0.33e/Å^3) and consistent with the estimate of electron density for the lipid head group. For DNA-NP layer we estimate $\frac{\rho_{NP}}{\rho_l}$ ~ 1.5, where ρ_{NP} is the maximum electron density of

the gold layer respectively. In addition to increase in the surface electron density we find increase in the interface thickness to ~ 10nm which yield DNA-NP layer thickness to ~ 7nm (after subtracting the thickness of the lipid layer ~ 3nm as determined from XRR for the bare lipid layer without NP. The estimate of the thickness of DNA-NP layer less than the diameter of NP particle (~8.8 ±0.8nm) along with asymmetric electron density profile, suggest strong interaction between lipid and DNA-NP layer[5]. In Figure S4c, we provide the various fit parameter for XRR data of different systems. We observed a subtle difference between the morphology of the DNA-NP and lipid layer at S_N and S_A states of the assembly. The high q region for S_A reveals higher amplitude of the oscillation, as compared to S_N. This corresponds to changes in the lipid/DNA-NP interface, as indicated by the *e*-density profile, which exhibits a higher contrast and a larger thickness for the lipid/DNA-NP layer (main text).

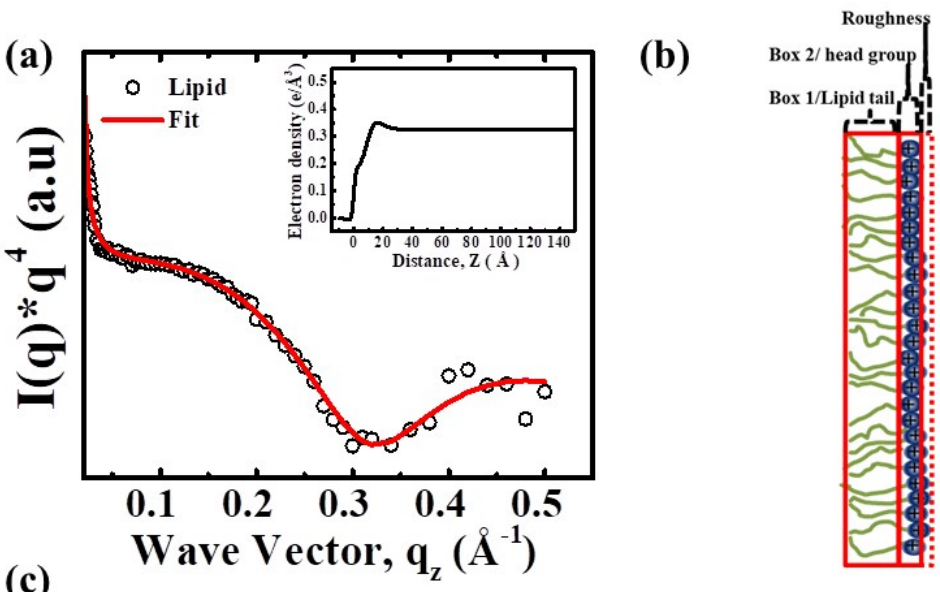

(c)

System	Layer Name	Thickness	SLD Real	SLD Imag	Roughness
Bare Lipid Layer	Lipid Tail	8.72	5.59	3e-08	2.3
	Lipid Head	2.3124	12.44	3e-08	3.94
	Interface Lipid/water	0.0000984	0.89	3e-08	10

System	Layer Name	Thickness	SLD Real	SLD Imag	Roughness
S_N	Lipid Tail	8.72	5.59	3e-08	2.3
	Lipid Head	2.31	12.44	3e-08	3.9
	Interface Lipid/water	0.00	0.09	3e-08	4.7
	DNA Layer	4.56	9.09	1e-06	5.0
	Gold nanoparticle	64.18	13.50	1e-06	4.7
	DNA/water interface	0.00	16.97	1e-06	6.7

System	Layer Name	Thickness	SLD Real	SLD Imag	Roughness
S_A	Lipid Tail	8.72	5.59	3e-08	2.3
	Lipid Head	2.31	12.44	3e-08	3.94
	Interface Lipid/water	1.00	0.49	3e-08	9.68
	DNA Layer	8.00	10.7	1e-06	5.01
	Gold nanoparticle	70.12	14.03	1e-06	4.22
	DNA/water interface	0.00	9.3	1e-06	14.28

Figure S4 (a) The XRR data for lipid monolayer along with fit. Inset: Electron density profile obtained from the fit as discussed in text. (b) Schematic demonstration of the box model used for fit in Igor using Motofit package for bare lipid layer. (c) The fitting parameters for different system as indicated.

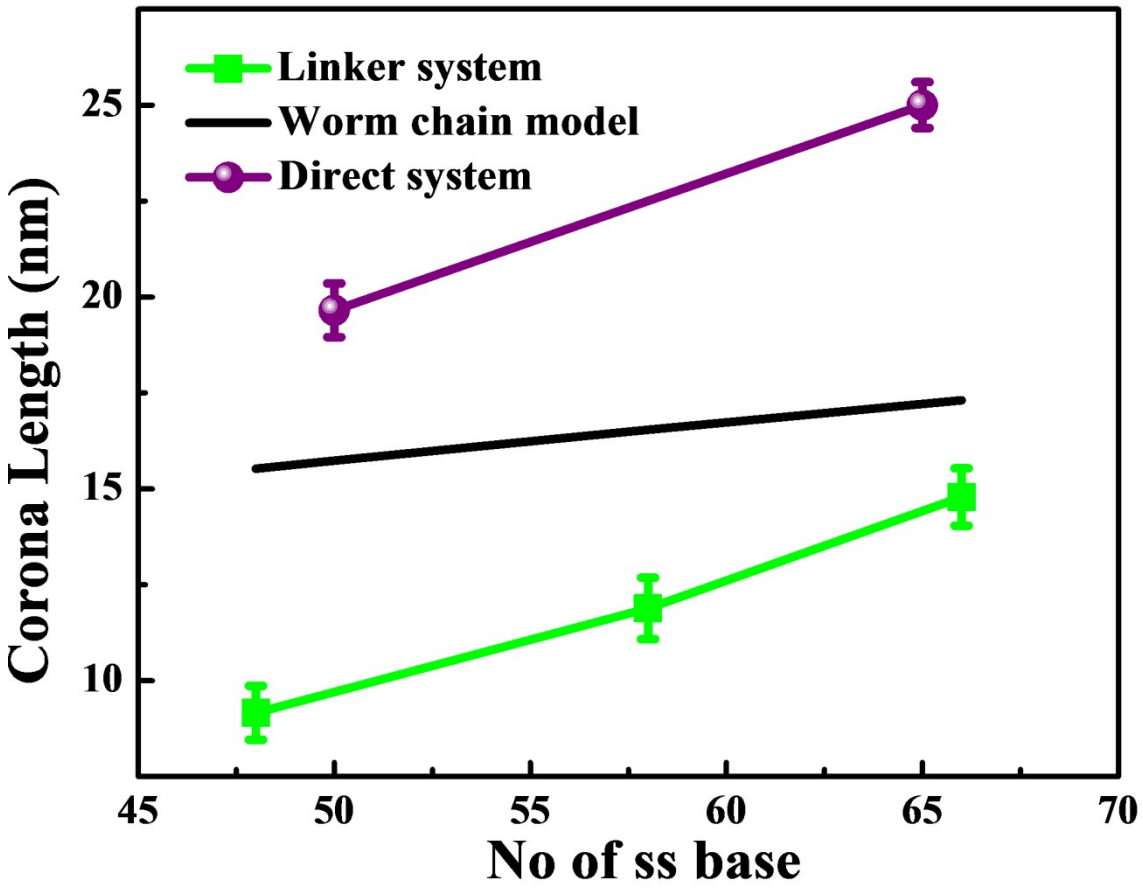

Figure S5. Comparison of the experimental data with the theoretical worm-chain model[6] for DNA functionalized nanoparticles that can be connected by direct DNA hybridization of complementary strands (∞) and for linker mediated pH driven *A*-motif formation (🕗).

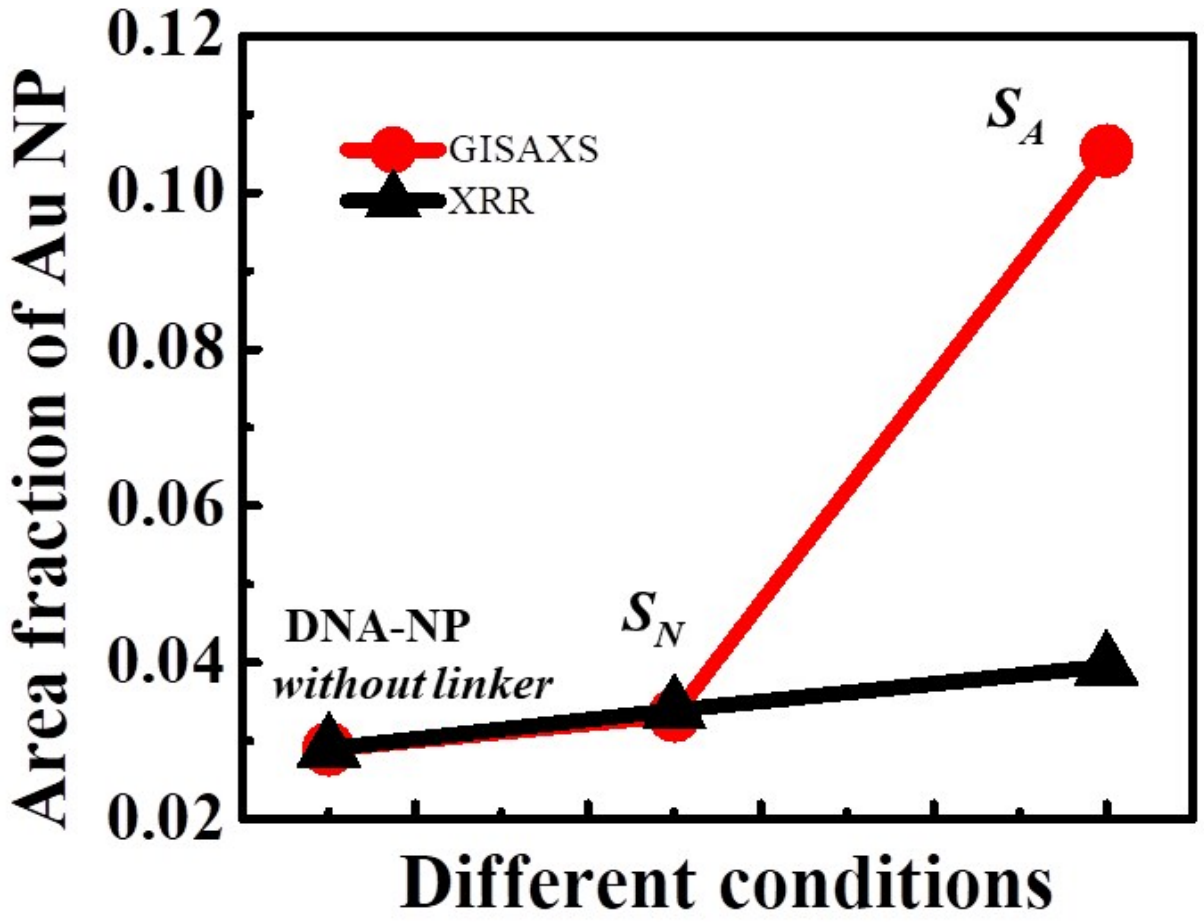

Figure S6. Area fraction occupied by gold nanoparticle at the interface under different conditions. At initial (DNA-NP in water, no linker attached), and S_A states, the estimates from GISXAS (ꝏ) and XRR (▲) are in good agreement, revealing the formation of homogeneous layer. However, at S_A, GISAXS result is an over estimation due to the presence of empty areas that arise because of the bond formation between pH activated linkers at the acidic conditions.

Scanning Electron Microscopy Measurements (SEM)

We have performed ex-situ SEM measurements on the DNA-NP monolayer to study the assembly structure. For such measurements we have used Silicon substrates were cleaned with Piranha solution to remove any surface contaminants. The surfaces of freshly cleaned substrates

were charged positively using layer-by-layer (LBL) deposition of polyelectrolytes. More specifically, firstly substrates were dip coated with solution of positively charged polymer, poly (diallyldimethylammonium chloride) (PDDA) of concentration 1 mg/ml for ~ 30 mins. After incubation for 30mins the substrates were rinsed several times with pure DI water. The alternate layer of negatively charged polymer, poly(acrylic acid) (PAA, 1 mg/ml) and PDDA layer were deposited by drop casting solution and incubation for ~ 15 mins followed by subsequent rinsing with clean water. To transfer the gold monolayer at the air/water interface the substrate was gently brought in contact with the monolayer from the top. The transferred monolayer were rinsed and dried under gentle airflow before the microscopy measurements. Shown below is an typical SEM image of the ex-situ 2D Au nanoparticle monolayer on silicon substrate.

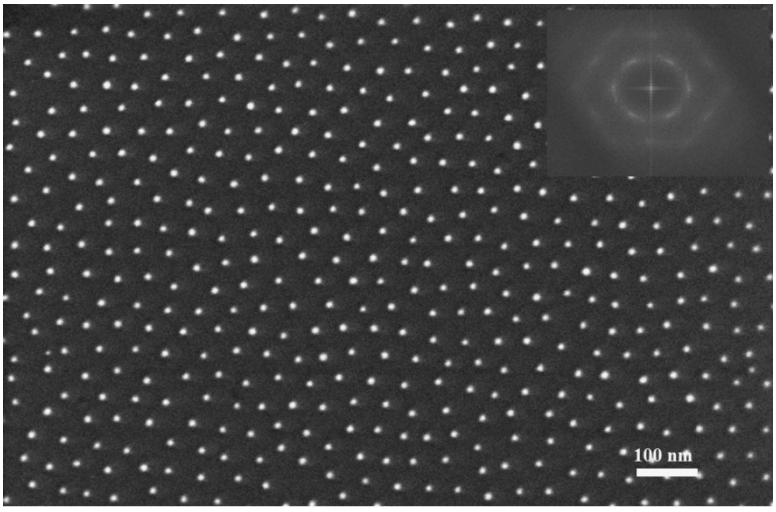

Figure S7. Typical ex-situ SEM image from DNA_NP layer transferred to solid substrate. The Fourier transform clearly indicates the formation of HCP lattice

References:

1. Kewalramani, S.; Wang, S. T.; Lin, Y. A.; Huong, G. N.; Wang, Q. A.; Fukuto, M.; Yang, L., Systematic approach to electrostatically induced 2D crystallization of nanoparticles at liquid interfaces. *Soft Matter* **2011,** *7* (3), 939-945.
2. Nykypanchuk, D.; Maye, M. M.; van der Lelie, D.; Gang, O., DNA-guided crystallization of colloidal nanoparticles. *Nature* **2008,** *451* (7178), 549-52.
3. Fukuto, M.; Wang, S. T.; Lohr, M. A.; Kewalramani, S.; Yang, L., Effects of surface ligand density on lipid-monolayer-mediated 2D assembly of proteins. *Soft Matter* **2010,** *6* (7), 1513-1519.
4. Nelson, A., Co-refinement of multiple-contrast neutron/X-ray reflectivity data using MOTOFIT. *J Appl Crystallogr* **2006,** *39*, 273-276.

5. Srivastava, S.; Nykypanchuk, D.; Fukuto, M.; Halverson, J. D.; Tkachenko, A. V.; Yager, K. G.; Gang, O., Two-Dimensional DNA-Programmable Assembly of Nanoparticles at Liquid Interfaces. *J Am Chem Soc* **2014,** *136* (23), 8323-8332.
6. Doi, M.; Edwards, S., *The Theory of Polymer Dynamics*. Oxford University Press: New York, 1998.